JOURNAL OF SOLID STATE CHEMISTRY 118, 367–371 (1995)

Relation between Electrical Properties and Cation–Anion–Cation Overlap in $Nd(Cr_{1-x}Mn_x)O_3$

Hideki Taguchi

Research Laboratory for Surface Science, Faculty of Science, Okayama University, Okayama 700, Japan

Received January 17, 1995; in revised form March 17, 1995; accepted March 17, 1995

Perovskite-type $Nd(Cr_{1-x}Mn_x)O_3$ was stoichiometrically synthesized in the range $0 \le x \le 0.6$ and has the orthorhombic $GdFeO_3$-type structure with space group *Pnma*. The average (Cr, Mn)–O distance and the effective magnetic moment (μ_{eff}) indicate that the Mn^{3+} ion is in a high-spin state with the $(d\varepsilon)^3(d\gamma)^1$ configuration. From the results of the electrical resistivity (ρ), $Nd(Cr_{1-x}Mn_x)O_3$ is a semiconductor and has a maximum ionization energy (ΔE) at $x = 0.2$. Rietveld analysis indicates that each (Cr, Mn)O_6 octahedron has little distortion and that the average angles for (Cr, Mn)–O(2)–(Cr, Mn) have a maximum value at $x = 0.2$, that is, the overlap between the cation $d\varepsilon$ and oxygen p_π orbitals plays an important role in the electrical properties of $Nd(Cr_{1-x}Mn_x)O_3$. © 1995 Academic Press, Inc.

INTRODUCTION

$NdCrO_3$ has an orthorhombic $GdFeO_3$-type structure with $a = 5.430$ Å, $b = 7.692$ Å, and $c = 5.488$ Å (1), and exhibits antiferromagnetism with a Néel temperature (T_N) of 224 K (2). The Cr^{3+} ions ($3d^3$) have the electron configuration $(d\varepsilon)^3(d\gamma)^0$ which is similar to that of the Mn^{4+} ions. From the temperature dependence of the electrical resistivity (ρ), $NdCrO_3$ exhibits a p-type semiconducting behavior above room temperature (1); the activation energy (E_a) calculated from the linear portion of the log ρ–$1000/T$ curve is ca. 0.28 eV (3).

$NdMnO_3$ also has the $GdFeO_3$-type structure with $a = 5.406$ Å, $b = 7.556$ Å, and $c = 5.789$ Å, and exhibits weak ferromagnetism with a Curie temperature (T_C) of 50 K (4). From the results of the magnetic measurement, the electron configuration of the Mn^{3+} ions ($3d^4$) is the high-spin state $(d\varepsilon)^3(d\gamma)^1$. According to Kamegashira and Miyazaki, $NdMnO_3$ shows nonstoichiometry, that is, the stoichiometric $NdMnO_3$ was obtained below log (P_{O_2}/Pa) = 1.0 and the cell volume of $NdMnO_{3+\delta}$ decreases linearly with increasing oxygen content (5). $NdMnO_{3+\delta}$ is a p-type semiconductor and the hole-hopping mechanism is dominant as in $LaMnO_3$ (5, 6).

Both the Cr^{3+} ions ($3d^3$) and the Mn^{3+} ions ($3d^4$) coexist in the $Nd(Cr_{1-x}Mn_x)O_3$ system. In the present study, $Nd(Cr_{1-x}Mn_x)O_3$ was synthesized to study its electrical properties, magnetic properties, and the structure refinement. These results will provide information regarding the cation–anion–cation overlap in the perovskite-type $Nd(Cr_{1-x}Mn_x)O_3$.

EXPERIMENTAL

$Nd(Cr_{1-x}Mn_x)O_3$ was prepared by a standard ceramic technique. Dried Nd_2O_3, Cr_2O_3, and MnO_2 powders were weighed in the appropriate proportions and milled for a few hours with acetone. After the mixed powders were dried at 373 K, they were calcined at 1173 K for a few hours in air, then fired 1623 K for 24 hr in air. In order to measure the electrical resistivities, the powders were pressed into a rod form under a pressure of 50 MPa, and the rod was sintered at 1623 K for 12 hr in air.

The phases of the samples were identified by X-ray powder diffraction (XRD) with monochromatic Cu$K\alpha$ radiation. The cell constants of the samples were determined from high-angle reflections with Si as an external standard. The structure refinement was carried out by Rietveld analysis of the XRD data with the "RIETAN" program written by Izumi (7). XRD data were collected by step scanning over an angular range of $20° \le 2\theta \le 100°$ in increments of $0.02°$ (2θ) with monochromatic Cu$K\alpha$ radiation. The electrical resistivity of the samples was measured in air by a standard four-electrode technique in the temperature range 300–1000 K. The magnetic susceptibility was measured by a magnetic torsion balance in the temperature range 80–703 K.

RESULTS AND DISCUSSION

XRD patterns of $Nd(Cr_{1-x}Mn_x)O_3$ ($0 \le x \le 1.0$) were completely indexed as the orthorhombic perovskite-type ($GdFeO_3$-type) structure. Figure 1 shows the relationship between the cell constants (a-, b-, and c-axes) and the composition. In Fig. 1, the cell constants of stoichiometric $NdMnO_3$ ($x = 1.0$) reported by Kamegashira and Miyazaki are also plotted as filled circles (5). In the range $0 \le x \le$

0022-4596/95 $12.00

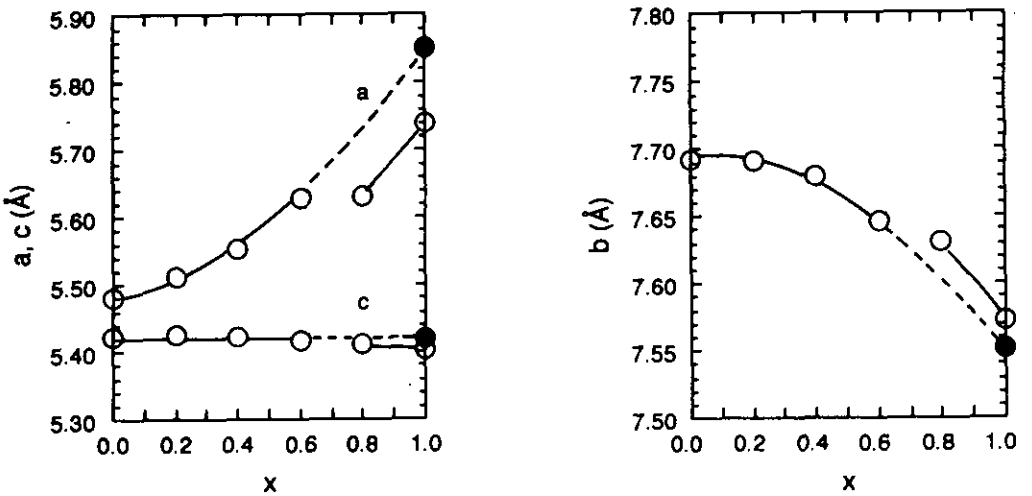

FIG. 1. Cell constants vs composition for the system $Nd(Cr_{1-x}Mn_x)O_3$. The filled circles indicate the values reported by Kamegashira and Miyazaki (5).

0.6, the a-axis increases and the c-axis is independent of x, while the b-axis decreases with increasing x. In the present study, owing to the synthesis of $NdMnO_3$ (x = 1.0) at 1623 K in air, the oxygen content is more than 3.0 and the cell constants extrapolated from the values in the range $0 \leq x \leq 0.6$ agree with those of stoichiometric $NdMnO_3$ (5).

Figure 2 shows the relationship between the cell volume (V) of $Nd(Cr_{1-x}Mn_x)O_3$ ($0 \leq x \leq 1.0$) and the composition. The cell volume of $NdCrO_3$ (x = 0) is 228.6 Å^3 and increases with increasing x. The cell volume of $NdMnO_3$ (x = 1.0), extrapolated from the values in the range $0 \leq x \leq 0.6$, agrees with the cell volume of stoichiometric $NdMnO_3$ (V = 239.5 Å^3) (5). From the results of Figs. 1 and 2, it is obvious that stoichiometric $Nd(Cr_{1-x}Mn_x)O_3$ was synthesized in the range $0 \leq x \leq 0.6$. In the present study, therefore, the magnetic properties and the electrical resistivity of $Nd(Cr_{1-x}Mn_x)O_3$ were measured in the range $0 \leq x \leq 0.6$. The ionic radii of a Cr^{3+} ion, a Mn^{3+} ion (low-spin state), and the Mn^{3+} ion (high-spin state) with a coordination number (CN) of 6 are 0.615, 0.58, and 0.65 Å, respectively (8). The increase in the cell volume is explained by the difference in the ionic radius between the Cr^{3+} and Mn^{3+} ions, and the Mn^{3+} ions must be in the high-spin state $(d\varepsilon)^3(d\gamma)^1$.

The temperature dependence of the inverse magnetic susceptibility ($1/\chi$) on $Nd(Cr_{1-x}Mn_x)O_3$ ($0 \leq x \leq 0.6$) is shown in Fig. 3. $NdCrO_3$ (x = 0) is antiferromagnetic with $T_N \approx 220$ K, while $Nd(Cr_{1-x}Mn_x)O_3$ ($0.2 \leq x \leq 0.6$) is

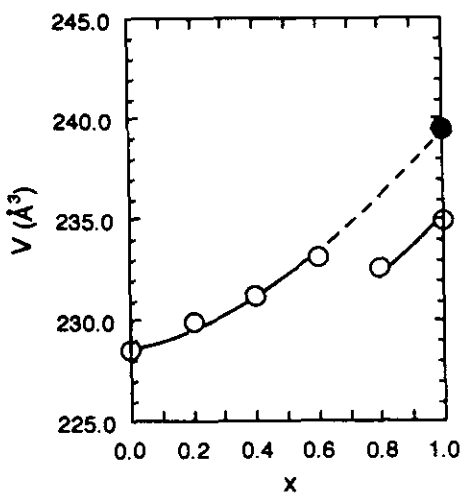

FIG. 2. Cell volume vs composition for the system $Nd(Cr_{1-x}Mn_x)O_3$. The filled circle indicates the value reported by Kamegashira and Miyazaki (5).

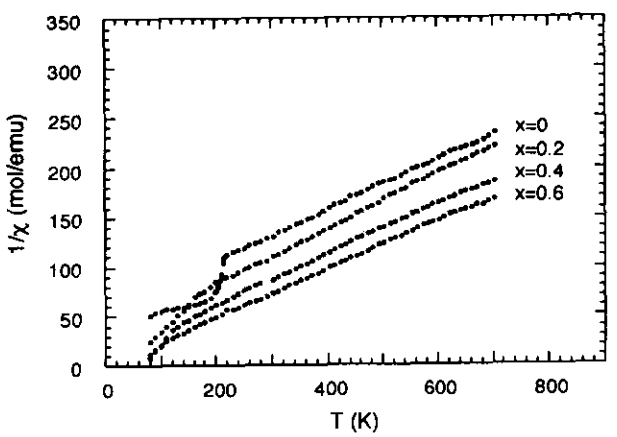

FIG. 3. Temperature dependence of the inverse magnetic susceptibility ($1/\chi$) for the system $Nd(Cr_{1-x}Mn_x)O_3$.

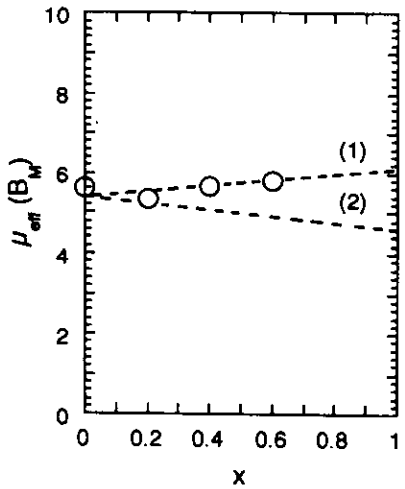

FIG. 4. Effective magnetic moment (μ_{eff}) vs composition for the system $Nd(Cr_{1-x}Mn_x)O_3$.

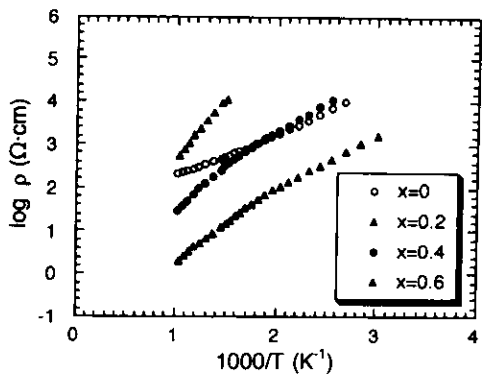

FIG. 5. Electrical resistivity (ρ) vs $1000/T$ for the system $Nd(Cr_{1-x}Mn_x)O_3$.

paramagnetic above 80 K. The $1/\chi$–T curves obey the Curie–Weiss law above 220 K, and the paramagnetic Curie temperature (T_θ) for $x = 0$, 0.2, 0.4, and 0.6 are ca. −216, −95, −55, and −8 K, respectively. The effective magnetic moment (μ_{eff}) of $Nd(Cr_{1-x}Mn_x)O_3$ calculated from the linear portion of the $1/\chi$–T curve increases with increasing x and is shown in Fig. 4. The theoretical μ_{eff} is calculated using the equation

$$\mu_{eff} = \sqrt{(1-x)\mu^2_{Cr^{3+}} + x\mu^2_{Mn^{3+}} + \mu^2_{Nd^{3+}}}, \quad [1]$$

where $\mu_{Cr^{3+}}$, $\mu_{Mn^{3+}}$, and $\mu_{Nd^{3+}}$ are the effective magnetic moments of the Cr^{3+} ion, the Mn^{3+} ion, and the Nd^{3+} ion, respectively (9). The spectroscopic splitting factors (g) of the Nd^{3+} ion and $\mu_{Nd^{3+}}$ are calculated using the equations (10)

$$g = 1 + \frac{J(J+1) + S(S+1) - L(L+1)}{2J(J+1)} \quad [2]$$

$$\mu_{Nd^{3+}} = g\sqrt{J(J+1)}. \quad [3]$$

The orbital angular momentum (L) is 6, the spin angular momentum (S) is 1.5, and the total angular momentum (J) is 4.5. Therefore, g is calculated to be 0.727 and $\mu_{Nd^{3+}}$ is 3.62. In Fig. 4, broken lines (1) and (2) indicate the theoretical values calculated for cases of both the high-spin and low-spin states of the Mn^{3+} ions; line (1) is the high-spin state $(d\varepsilon)^3(d\gamma)^1$ and line (2) is the low-spin state $(d\varepsilon)^4(d\gamma)^0$. From the results of Fig. 4, it is obvious that the spin state of the Mn^{3+} ions in $Nd(Cr_{1-x}Mn_x)O_3$ is high.

The relationship between the electrical resistivity (ρ) of $Nd(Cr_{1-x}Mn_x)O_3$ and the reciprocal temperature ($1000/T$) is shown in Fig. 5. The decrease in log ρ with increasing temperature indicates that $Nd(Cr_{1-x}Mn_x)O_3$ is a semiconductor above room temperature. The ionization energy gap (ΔE) between the valence band (E_V) and the acceptor level (E_A) is calculated from the linear portion of log ρ–$1000/T$ curves, and the relationship between ΔE and the composition is shown in Fig. 6. Although $3d$ electrons in $Nd(Cr_{1-x}Mn_x)O_3$ increase with the substitution of Cr^{3+} ions ($3d^3$) by Mn^{3+} ions ($3d^4$), ΔE of $NdCrO_3$ ($x = 0$) is ca. 0.45 eV and has a maximum value (ca. 1.15 eV) at $x = 0.2$.

The structure refinement of $Nd(Cr_{1-x}Mn_x)O_3$ ($0 \le x \le 0.6$) was carried out by Rietveld analysis of XRD data. $Nd(Cr_{1-x}Mn_x)O_3$ has an orthorhombic $GdFeO_3$-type structure with space group *Pnma* (11). In the present study, isotropic thermal parameters (B) for Nd, Cr, Mn, O(1), and O(2) ions were fixed at 0.3 Å^2 for all samples. Refined structural parameters and residuals, R_{WP}, R_I, and

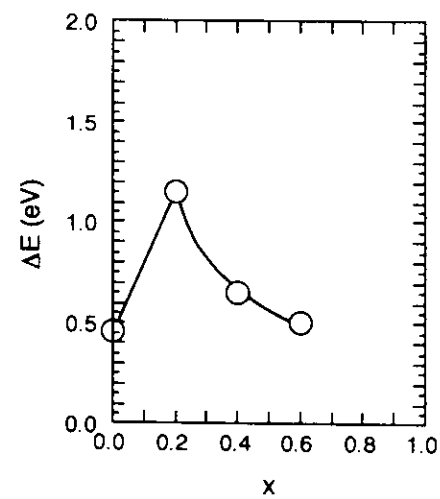

FIG. 6. Ionization energy (ΔE) vs composition for the system $Nd(Cr_{1-x}Mn_x)O_3$.

TABLE 1
Refined Structure Parameters for $Nd(Cr_{1-x}Mn_x)O_3$

$x = 0.0$	$a = 5.4798(1)$ Å	$b = 7.6918(2)$ Å		$c = 5.4208(1)$ Å	
	$R_{WP} = 12.69\%$	$R_I = 2.01\%$		$R_F = 1.29\%$	
Atom	Position	x	y	z	B
Nd	4(*c*)	0.041(1)	0.25	−0.008(1)	0.3
Cr	4(*b*)	0	0	0.5	0.3
O(1)	4(*c*)	0.484(4)	0.25	0.082(6)	0.3
O(2)	8(*d*)	0.292(4)	0.041(3)	−0.289(4)	0.3
$x = 0.2$	$a = 5.5110(2)$ Å	$b = 7.6905(3)$ Å		$c = 5.4254(2)$ Å	
	$R_{WP} = 16.02\%$	$R_I = 2.57\%$		$R_F = 1.86\%$	
Atom	Position	x	y	z	B
Nd	4(*c*)	0.045(5)	0.25	−0.009(1)	0.3
Cr, Mn	4(*b*)	0	0	0.5	0.3
O(1)	4(*c*)	0.487(6)	0.25	0.097(8)	0.3
O(2)	8(*d*)	0.290(5)	0.037(4)	−0.285(5)	0.3
$x = 0.4$	$a = 5.5548(1)$ Å	$b = 7.6795(2)$ Å		$c = 5.4218(1)$ Å	
	$R_{WP} = 16.30\%$	$R_I = 2.79\%$		$R_F = 2.04\%$	
Atom	Position	x	y	z	B
Nd	4(*c*)	0.048(1)	0.25	−0.010(1)	0.3
Cr, Mn	4(*b*)	0	0	0.5	0.3
O(1)	4(*c*)	0.485(6)	0.25	0.094(7)	0.3
O(2)	8(*d*)	0.292(5)	0.041(4)	−0.286(5)	0.3
$x = 0.6$	$a = 5.6272(2)$ Å	$b = 7.6468(2)$ Å		$c = 5.4181(2)$ Å	
	$R_{WP} = 19.56\%$	$R_I = 4.24\%$		$R_F = 2.61\%$	
Atom	Position	x	y	z	B
Nd	4(*c*)	0.054(1)	0.25	−0.011(1)	0.3
Cr, Mn	4(*b*)	0	0	0.5	0.3
O(1)	4(*c*)	0.479(8)	0.25	0.093(8)	0.3
O(2)	8(*d*)	0.301(6)	0.044(4)	−0.282(7)	0.3

R_F are listed in Table 1. R_{WP}, R_I, and R_F are the residuals for the weighted pattern, the integrated intensity, and the structure factor, respectively. The final R_F of all samples was less than 2.61%, and the low R_F suggests that the structural model for $Nd(Cr_{1-x}Mn_x)O_3$ is reasonable.

In the orthorhombic $GdFeO_3$-type structure, A-site cations (Nd ions) coordinate with 12 anions: 4 O(1) and 8 O(2) ions. B-site cations (Cr and Mn ions) coordinate with 6 anions: 2 O(1) and 4 O(2) ions. The average (Cr, Mn)–O distance of $Nd(Cr_{1-x}Mn_x)O_3$ was calculated from the refined structural parameters and is shown in Fig. 7. The average Cr–O distance of $NdCrO_3$ ($x = 0$) is ca. 1.977 ± 0.014 Å. Because the ionic radius of the Mn^{3+} ion with the high-spin state is larger than the ionic radii of the Cr^{3+} ion (8), the average (Cr, Mn)–O distance increases linearly with increasing x. The angles for O–(Cr, Mn)–O and (Cr, Mn)–O–(Cr, Mn) of $Nd(Cr_{1-x}Mn_x)O_3$ are calculated from the refined structural parameters. The average angles for O(1)–(Cr, Mn)–O(1), O(1)–(Cr, Mn)–O(2), and O(2)–(Cr, Mn)–O(2) are 180, 90, and 90 or 180°, respectively. From the results of the average (Cr, Mn)–O distances and the average angles for O–(Cr, Mn)–O, it is obvious that each (Cr, Mn)O_6 octahedron has little distortion. The average angles for (Cr, Mn)–O(1)–(Cr, Mn) and (Cr, Mn)–O(2)–(Cr, Mn) are less than 180° and are shown in Fig. 8. The average angle for (Cr, Mn)–O(1)–(Cr, Mn) decreases in the range $0 \leq x \leq 0.2$; it is independent of composition in the range $0.2 \leq x \leq 0.6$. On the other hand, the average angle for (Cr, Mn)–O(2)–(Cr, Mn) in-

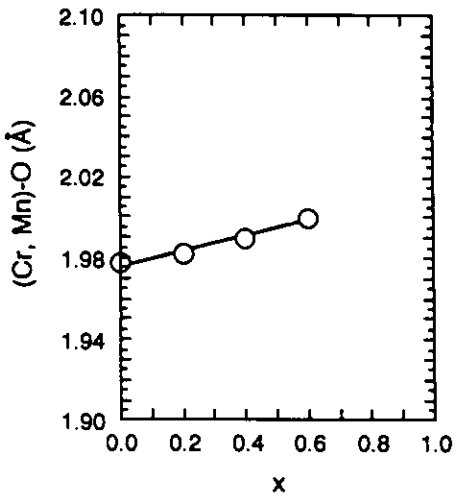

FIG. 7. Average (Cr, Mn)–O distance vs composition for the system $Nd(Cr_{1-x}Mn_x)O_3$.

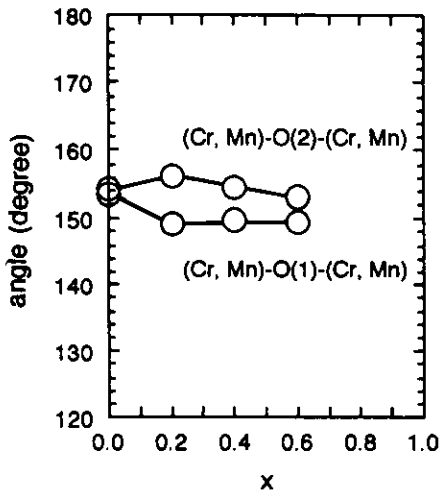

FIG. 8. Angles for (Cr, Mn)–O(1)–(Cr, Mn) and (Cr, Mn)–O(2)–(Cr, Mn) vs composition for the system $Nd(Cr_{1-x}Mn_x)O_3$.

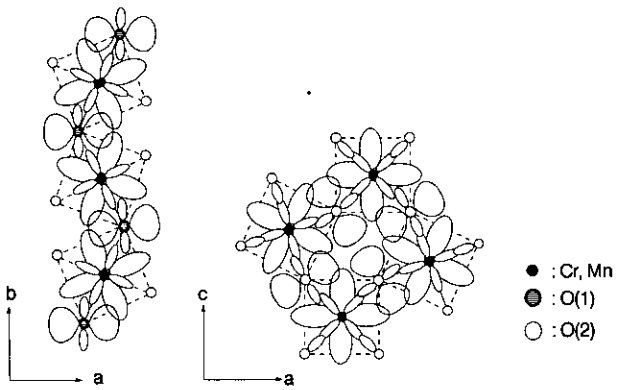

FIG. 9. Crystal structure of $Nd(Cr_{1-x}Mn_x)O_3$.

creases and has its maximum value (156.3 ± 1.5°) at x = 0.2, and then decreases linearly with increasing x.

Figure 9 shows the crystal structure of $Nd(Cr_{1-x}Mn_x)O_3$. The (Cr, Mn)O_6 octahedron connects at O(1) or O(2) of the other's (Cr, Mn)O_6 octahedron. The Cr^{3+} ions have the electron configuration $(d\varepsilon)^3(d\gamma)^0$ and the Mn^{3+} ions have the electron configuration $(d\varepsilon)^3(d\gamma)^1$ in $Nd(Cr_{1-x}Mn_x)O_3$. Therefore, there are two kinds of cation–anion–cation overlap; one is an overlap (π bond) between the cation $d\varepsilon$ and oxygen p_π orbitals, and the other is the overlap (σ bond) between the cation $d\gamma$ and oxygen p_σ orbitals. According to the one electron energy diagram for $LaCrO_3$, the three $3d$ electrons of the Cr^{3+} ion are all localized and the Fermi level lies between the filled $d\varepsilon^*$ levels and the narrow $d\gamma^*$ levels (12). Although the activation energy (E_a) calculated from the electronic spectra is ca. 1.0 eV (13), the measured E_a is smaller than 1.0 eV and Rao *et al.* proposed that the Cr^{4+} ions present as a result of impurities or native defects give rise to p-type extrinsic conduction in $LaCrO_3$ (14). Owing to the high ΔE of semiconducting $Nd(Cr_{1-x}Mn_x)O$, it is considered that both the $d\varepsilon^*$ and $d\gamma^*$ levels are localized and narrow; the cation–anion–cation overlap integrals (Δ^π_{cac} for π bond and Δ^σ_{cac} for σ bond) are smaller than the critical overlap integral (Δ_c); $\Delta^\pi_{cac} < \Delta^\sigma_{cac} < \Delta_c$ (15). The $d\varepsilon^*$ level is fully filled by three $3d$ electrons and the $d\gamma^*$ level is partly filled. The intra-atomic exchange (Δ_{ex}) between the $d\varepsilon^*$-α and $d\varepsilon^*$-β levels is larger than the crystal-field splitting (10 Dq) between the $d\varepsilon^*$ and $d\gamma^*$ levels. From a geometrical arrangement between the cation $d\gamma$ and oxygen p_σ orbitals, it is obvious that σ bonding is strong where the average angle for (Cr, Mn)–O(1)–(Cr, Mn) is 180°, and the decrease in the average angle for (Cr, Mn)–O(1)–(Cr, Mn) from 180° weakens σ bonding. On the other hand, the overlap between the cation $d\varepsilon$ and oxygen p_π orbitals increases with the deviation of the average angle for (Cr, Mn)–O(2)–(Cr, Mn) from 180°, that is, π bonding becomes stronger. The number of σ bonding, π bonding, and $3d$ electrons is generally considered to be the important factor in the electrical properties of $Nd(Cr_{1-x}Mn_x)O_3$. The linear increase in the number of $3d$ electrons or the monotonic decrease in σ bonding with increasing x cannot explain the maximum ΔE at x = 0.2. As seen in Fig. 8, the increase in the average angle for (Cr, Mn)–O(2)–(Cr, Mn) at x = 0.2 weakens π bonding. Therefore, it is considered that electron transfer through π bonding decreases, and $Nd(Cr_{1-x}Mn_x)O_3$ has the maximum ΔE at x = 0.2.

CONCLUSION

From the cell constants and the cell volume, stoichiometric $Nd(Cr_{1-x}Mn_x)O_3$ was synthesized in the range $0 \leq x \leq 0.6$. The increases in the average (Cr, Mn)–O distance and μ_{eff} indicate that the Mn^{3+} ion is in the high-spin state $(d\varepsilon)^3(d\gamma)^1$. The temperature dependence of log ρ indicates that $Nd(Cr_{1-x}Mn_x)O_3$ is semiconductive with maximum ΔE at x = 0.2, and this maximum value corresponds to the variation in the average angles for (Cr, Mn)–O(2)–(Cr, Mn). Therefore, it is considered that the electrical properties of $Nd(Cr_{1-x}Mn_x)O_3$ depend on the overlap between the cation $d\varepsilon$ and oxygen p_π orbitals.

ACKNOWLEDGMENT

The author expresses his thanks to Dr. H. Kido, Osaka Municipal Technical Institute for the magnetic measurements.

REFERENCES

1. T. Arakawa, S. Tsuchi-Ya, and J. Shiokawa, *Mater. Res. Bull.* **16,** 97 (1981).
2. J. B. Goodenough and J. M. Longo, "Landolt-Boernstein, Numerical Data and Functional Relationships in Science and Technology. New Series, Group 3, Vol. 4, Magnetic and Other Properties of Oxides and Related Compounds," (K. H. Hellwege, Ed.), p. 228. Springer-Verlag, New York, 1971.
3. H. Taguchi, M. Nagao, and Y. Takeda, *J. Solid State Chem.* **114,** 236 (1995).
4. T. Arakawa, A. Yoshida, and J. Shiokawa, *Mater. Res. Bull.* **15,** 269 (1980).
5. N. Kamegashira and Y. Miyazaki, *Mater. Res. Bull.* **19,** 1201 (1984).
6. J. B. Goodenough, "Progress in Solid State Chemistry," (H. Reiss, Ed.), Vol. 5, p. 145, Pergamon, Oxford 1971.
7. F. Izumi, *Nippon Kesho Gakkaishi* **27,** 23 (1985). [in Japanese]
8. R. D. Shannon and C. T. Prewitt, *Acta Crystallogr. Sect. B* **25,** 925 (1969).
9. T. Shin-Ike, T. Sakai, G. Adachi, and J. Shiokawa, *Mater. Res. Bull.* **12,** 831 (1977).
10. A. J. Dekker, "Solid State Physics," p. 450. Prentice-Hall, New York 1970.
11. K. R. Poeppelmeier, M. E. Leonowicz, J. C. Scanlon, and W. B. Yelon, *J. Solid State Chem.* **45,** 71 (1982).
12. J. B. Goodenough, *J. Appl. Phys.* **37,** 1415 (1966).
13. J. S. Ruiz, A. M. Anthony, and M. Foex, *Compt. Rend. B* **264,** 1271 (1967).
14. G. V. Rao, B. M. Wanklyn, and C. N. R. Rao, *J. Phys. Chem. Solids* **32,** 345 (1971).
15. J. B. Goodenough, *Czech. J. Phys. B* **17,** 304 (1967).